coefficient of left ventricular cavity was given by the myocardial static blood volume image and was also used to determine myocardial blood flow [Iida et al. 1998]. After 12-15 minutes, to allow for decay of $^{15}O$-radioactivity to background levels, transmission scanning was undertaken over 10 minutes. Then, $H_2{}^{15}O$ PET studies were performed at rest, and under hypercapnea and hypocapnea. The order of the studies was rest, hypercapnea, and hypocapnea studies in 7 subjects, and rest, hypocapnea, and hypercapnea studies in 6 subjects. The intervals between $H_2{}^{15}O$ PET studies were at least 15 minutes to allow the decay of radioactivity. Following the continuous intravenous infusion of $H_2{}^{15}O$ (1.1-1.4 GBq) over 2 minutes, 180-sec static imaging of the brain and 360-sec dynamic imaging of the heart were commenced. The dynamic data of the heart consisted of twelve 5- seconds frames, eight 15-seconds frames, and six 30- seconds frames. Hypercapnea was achieved by inhalation of 7% $CO_2$ gas, beginning 1 minute before $^{15}O$-water injection and continuing until the end of the imaging of the heart. Hypocapnea was induced by hyperventilation. Three arterial blood samples were taken during each PET scan to measure arterial carbon dioxide tension and pH.

**Data Analysis**

Cerebral blood flow images were generated from the PET data as described previously [Iida et al. 1998], and a region of interest for the inside of the brain contour was drawn on a slice of the cerebral blood flow image that was at the level of the basal ganglia. The region of interest was determined on an image obtained at rest and applied to images obtained under stress conditions. The mean cerebral blood flow in the region of interest was calculated from $^{15}O$-$H_2O$ autoradiography method [Raichle ME et al. 1983] and used for the following analyses. The percent change in cerebral blood flow at hypercapnea was defined as 100 × (cerebral blood flow at hypercapnea - cerebral blood flow at rest) / cerebral blood flow at rest, and cerebral blood flow responsiveness to hypercapnea was calculated as percent change in cerebral blood flow at hypercapnea divided by arterial carbon dioxide tension at hypercapnea minus arterial carbon dioxide tension at rest. The percent change in cerebral blood flow at hypocapnea and cerebral blood flow responsiveness to hypocapnea were determined using similar calculations, but using hypocapnea values instead.

The region of interests for the left ventricular cavity and the whole anterolateral wall

of the left ventricle at mid ventricular level were drawn on a slice of the short-axis myocardial images. The region of interests for the image at rest were copied on the myocardial images under the stress conditions. The myocardial blood flow value was estimated using the regions of interests according to a previously validated method [Iida et al. 1998]. In summary, myocardial blood flow was calculated using a non-linear least squares fitting technique of the left ventricular tissue and arterial $^{15}O$-$H_2O$ time activity curves [Iida H et al. 1988]. The input function was non-invasively determined from the time activity curve of left ventricular cavity [Iida H et al. 1992]. Time activity curve of the left ventricular cavity and that of the myocardial wall were fitted to the previously demonstrated tracer kinetic model equations to determine myocardial blood flow [Iida et al. 1998]. The percent change in myocardial blood flow at hypercapnea was defined as 100 × (myocardial blood flow during hypercapnea - myocardial blood flow at rest) / myocardial blood flow at rest, and myocardial blood flow responsiveness to hypercapnea was calculated as percent change in myocardial blood flow during hypercapnea divided by arterial carbon dioxide tension under hypercapnea minus arterial carbon dioxide tension at rest. The percent change in myocardial blood flow during hypocapnea and myocardial blood flow responsiveness to hypocapnea were determined using similar calculations but using hypocapnea values instead. In addition, normalized myocardial blood flow was calculated for the rate pressure product by the equation:

Normalized myocardial blood flow = 10000 × myocardial blood flow / rate pressure product, and percent change in normalized myocardial blood flow and normalized myocardial blood flow responsiveness were calculated.

**Statistical Analysis**

Values were expressed as the mean ± standard deviation. Comparisons were made by one-way analysis of variance followed by Fisher's least significant difference tests for parametric distributions and Kruskal-Wallis test followed by Scheffe's test for nonparametric distributions. A P value $< 0.05$ was considered statistically significant.

Results

**Hemodynamics**

Blood pressures, heart rate, rate pressure product, arterial carbon dioxide tension and pH are summarized in Table 1. Blood pressures were measured in the thigh because arteries and veins in both arms were cannulated. Since the blood pressure measured in the thighs were on average 25 mmHg higher than those measured in the arms in our institution, blood pressures in the thigh were considered to be within normal range. Electrocardiogram findings under hypercapnea or hypocapnea did not change compared with those at rest. Arterial carbon dioxide tension significantly decreased during hypocapnea and significantly increased during hypercapnea. Blood pressures significantly increased during hypercapnea but remained unchanged during hypocapnea. Rate pressure product did not change significantly during hypocapnea but significantly increased during hypercapnea.

**Cerebral blood flow**

Cerebral blood flow significantly decreased during hypocapnea and significantly increased during hypercapnea (Table2). The change in cerebral blood flow caused by hypocapnea was -32.2 percent ± 11.3 percent, and the cerebral blood flow responsiveness to hypocapnea was 3.0 ± 1.1 percent /mmHg. The change in cerebral blood flow caused by hypercapnea was 21.0 percent ± 15.5 percent, and the cerebral blood flow responsiveness to hypercapnea was 8.2 ± 5.3 percent /mmHg.

**Myocardial blood flow**

Hypocapnea caused a significant reduction in myocardial blood flow from baseline (Table 2). The percent change in myocardial blood flow caused by hypocapnea was -29.3 percent ± 15.1 percent, and the myocardial blood flow responsiveness to hypocapnea was 3.5 ± 3.0 percent /mmHg. Normalization for rate pressure product did not alter the percent change (- 30.4 percent ± 16.5 percent) and responsiveness (-2.2 ± 11.2 percent /mmHg) substantially. Under hypocapnea, the percent changes in cerebral blood flow, myocardial blood flow, and normalized myocardial blood flow were not significantly different compared with baseline. There were no significant differences in the responsiveness to hypocapnea between cerebral blood flow, myocardial blood flow, and normalized myocardial blood flow.

Hypercapnea significantly increased myocardial blood flow. The percent change in myocardial blood flow caused by hypercapnea was 12.5 percent ± 15.6 percent, and the myocardial blood flow responsiveness to hypercapnea was 5.2 ± 9.9 percent /mmHg. However, the increase in myocardial blood flow disappeared after normalization for rate pressure product. The change in normalized myocardial blood flow under hypercapnea was -2.2 percent ± 11.2 percent, and the normalized myocardial blood flow responsiveness to hypercapnea was -1.7 ± 8.8 percent /mmHg. As for hypercapnea, the percent change in normalized myocardial blood flow was significantly smaller than the change in cerebral blood flow ($p < 0.05$), and the normalized myocardial blood flow responsiveness was significantly smaller than cerebral blood flow responsiveness ($p < 0.05$).

**Discussion**

We simultaneously measured myocardial blood flow and cerebral blood flow at rest, during hypocapnea, and during hypercapnea in healthy elderly men. During hypocapnea, cerebral blood flow was reduced significantly as expected, and myocardial blood flow also diminished significantly to a similar magnitude. Rate pressure product did not change significantly from baseline, and myocardial blood flow normalized for rate pressure product also decreased. These results indicate that hypocapnea depresses myocardial blood flow, independently of cardiac workload, in healthy elderly men. The responsiveness to hypocapnea was similar between cerebral blood flow and myocardial blood flow, suggesting that hypocapnea can induce vasoconstriction in both heart and brain in healthy elderly men.

Several studies of coronary vascular response to hypocapnea using experimental animals have been reported however, the results were inconsistent [Feinberg 1960, Love 1965, Case 1976]. In a study of humans **with** negligible coronary artery disease, hypocapnea with 30.6 percent reduction in arterial carbon dioxide tension resulted in a significant 30.3 percent reduction in myocardial blood flow with a wide range of variability [Rowe 1962]. The present results are consistent with these previous studies. However, in studies of patients with coronary artery disease, hypocapnea resulted in a mild but significant 12 percent reduction in myocardial blood flow [Neill & Hattenhauer 1975] or did not change significantly [Wilson et al. 1981, Kazmaier et al. 1998]. Therefore, myocardial blood flow response to hypocapnea is likely to be different between normal subjects and patients with coronary artery disease. Since myocardial blood flow response to hypocapnea did not differentiate regions with myocardial ischemia from regions of non-ischemic myocardium in these studies of coronary artery disease, further study is required to clarify whether myocardial blood flow response to hypocapnea would differ between ischemic myocardium and non-ischemic myocardium.

Myocardial blood flow response to hypercapnea remains controversial. A number of experimental animal studies showed that hypercapnea did not increase myocardial blood flow [Feinberg et al. 1960, Love et al. 1965, van den Bos et al. 1979], whereas other studies showed that hypercapnea could increase myocardial blood flow [Case & Greenberg 1975, Powers et al. 1986]. In a study of anesthetized patients with coronary artery disease before

surgery, elevation of arterial carbon dioxide tension (+10 mmHg) resulted in a 15 percent increase in myocardial blood flow [Kazmaier et al. 1998]. However, the study did not estimate normalized myocardial blood flow to exclude the influence of cardiac workload on myocardial blood flow measurement [Kazmaier et al. 1998]. In this study, hypercapnea significantly increased myocardial blood flow and cerebral blood flow but not normalized myocardial blood flow with rate pressure product in healthy elderly men. Myocardial blood flow responsiveness to hypercapnea was significantly lower than that in cerebral blood flow when myocardial blood flow was normalized with respect to rate pressure product. Increase in cardiac workload under hypercapnea could explain an increase in myocardial blood flow. However, hypercapnea did not have an additional direct effect to increase myocardial blood flow independent of an elevation in cardiac workload under mild hypercapnea. Since myocardial blood flow responsiveness to hypercapnea was significantly lower than that in cerebral blood flow when myocardial blood flow was normalized with respect to cardiac workload, vascular responsiveness to hypercapnea is expected to be different between heart and brain. In this study, the magnitude of increase in arterial carbon dioxide tension during hypercapnea was small (3 mmHg), contrasting with the magnitude of decrease in arterial carbon dioxide tension during hypocapnea (11 mmHg). Such difference in the magnitude of changes in arterial carbon dioxide tension may explain why hypocapnea was effective to decrease the normalized myocardial blood flow but hypercapnea had no effect to increase the normalized myocardial blood flow. However, even under such very small increase in carbon dioxide tension, significantly elevated myocardial blood flow without normalization in response to an increase in cardiac workload was seen. Therefore, the importance of the carbon dioxide tension changes in determining the response of heart and brain perfusion could be discussed more than is presently done. To resolve such issues, much stronger hypercapneic stress test at different hypercapnic levels to increase arterial carbon dioxide tension is required to clarify whether hypercapnea directly increases myocardial blood flow independent of an increase in cardiac workload. Use of beta-blockers to exclude an influence of increase in cardiac workload for the myocardial blood flow measurement during hypercapnea [van den Bos et al. 1979, Powers et al. 1986] would also be helpful to understand myocardial blood

flow responsiveness to hypercapnea. For future studies, it is of interest to test the effect of normalization with both cardiac workload and arterial carbon dioxide tension changes on the studies of myocardial blood flow.

## Conclusion

In normal elderly men, hypocapnea produces similar vasoconstriction in both heart and brain. Mild hpercapnea increased cerebral blood flow but did not have an additional effect to dilate coronary arteries beyond the expected range in response to an increase in cardiac workload.

ACKNOWLEDGMENTS

This work was supported by grants from the Research Institute of Brain and Blood Vessels, Akita, Japan. We are grateful to Dr. T. Komaru (Tohoku University) for helpful discussions. The technical assistance for the PET experiments by the members of the Research Institute of Brain and Blood Vessels, Akita, Japan, is also gratefully acknowledged.

**Conflict of interest**

No conflict of interest exists in connection with this article.

References

Case, RB. & Greenberg, H. 1976. The response of canine coronary vascular resistance to local alterations in coronary arterial P CO2. *Circ Res* **39**, 558-66.

Feinberg, H., Gerola, A. & Katz, LN. 1960. Effect of changes in blood CO2 level on coronary flow and myocardial O2 consumption. *Am J Physiol* **199**, 349-354.

Iida, H., Kanno, I., Takahashi, A., Miura, S., Murakami, M., Takahashi, K., Ono, Y., Shishido, F., Inugami, A., Tamura, N., & Tomura, N. 1988. Measurement of absolute myocardial blood flow with H215O and dynamic positron-emission tomography. Strategy for quantification in relation to the partial-volume effect. *Circulation* **78**,104-115.

Iida, H., Miura, S., Shoji, Y., Ogawa, T., Kado, H., Narita, Y., Hatazawa, J., Eberl, S., Kanno, I. & Uemura, K. 1998. Non-invasive quantitation of CBF using oxygen-15-water and a dual-PET system. *J Nucl Med* **39**, 1789-1798.

Iida, H., Rhodes, CG., de Silva, R., Araujo, LI., Bloomfield, PM., Lammertsma, AA., & Jones, T. 1992. Use of the left ventricular time-activity curve as a noninvasive input function in dynamic oxygen-15-water positron emission tomography. J Nucl Med **33**,1669-1677.

Ito, H., Kinoshita, T., Tamura, Y., Yokoyama, I. & Iida, H. 2000. Effect of intravenous dipyridamole on cerebral blood flow in humans. A PET Study. *Stroke* **30**, 1616-1620.

Ito, H., Yokoyama, I., Iida, H., Kinoshita, T., Hatazawa, J., Shimosegawa, E., Okudera, T. & Kanno, I. 2000. Regional differences in cerebral vascular response to PaCO2 changes in humans measured by PET. *J Cerebral Blood Flow and Metab* **20**, 1264-1270.

Ito, H., Yokoyama, I., Tamura, Y., Kinoshita, T., Hatazawa, J., Kawashima, R. & Iida, H. 2002. Regional changes in human cerebral blood flow during dipyridamole stress: Neural activation in the thalamus and prefrontal cortex. Neuroimage **16**, 788-793.

Kazmaier, S., Weyland, A., Buhre, W., Stephan, H., Rieke, H., Filoda, K. & Sonntag, H. Effects of respiratory alkalosis and acidosis on myocardial blood flow and metabolism in patients with coronary artery disease. *Anesthesiology* **89**, 831-837.

Kety, SS. & Schmidt, CF. 1948. The effects of altered arterial tensions of carbon dioxide and oxygen on cerebral blood flow and cerebral oxygen consumption of normal young men. *J Clin Invest* **27**, 484-492.

Kuwabara, Y., Ichiya, Y., Sasaki, M., Yoshida, T., Masuda, K., Matsushima, T. & Fukui, M. 1997. Response to hypercapnia in moyamoya disease. Cerebrovascular response to hypercapnia in pediatric and adult patients with moyamoya disease. *Stroke* **28**, 701-707.

Love, WD., Tyler, MD., Abraham, RE. & Munford, RS. 1965. Effects of O2, CO2, and drugs on estimating coronary blood flow from Rb86 clearance. *Am J Physiol* **208**, 1206-1210.

Neill, WA. & Hattenhauer, M. 1975. Impairment of myocardial O2 supply due to hyperventilation. *Circulation* **52**, 854-858.

Powers, ER., Bannerman, KS., Fitz-James, I., & Cannon, PJ. 1986. Effect of elevations of coronary artery partial pressure of carbon dioxide (PCO2) on coronary blood flow. *J Am Coll Cardiol* **8**, 1175-1181.

Raichle, ME., Martin, WRW., Herscovitch, P., Mintun, MA., & Markham, J. 1983. Brain blood flow measured with intravenous H2(15)O. II. Implementation and validation. *J Nucl Med* **24**, 790-798.

Rowe, GG., Castillo, CA. & Crumpton, CW. 1962. Effects of hyperventilation on systemic and coronary hemodynamics. *Am Heart J* **63**, 67-77.

Shimosegawa, E., Kanno, I., Hatazawa, J., Fujita, H., Iida, H., Miura, S., Murakami, M., Inugami, A., Ogawa, T., Itoh, H., Okudera, T. & Umemura, K. 1995. Photic stimulation study of changing the arterial partial pressure level of carbon dioxide. *J Cereb Blood Flow Metab* **15**, 111-114.

van den Bos, GC., Drake, AJ. & Noble, MI. 1979. The effect of carbon dioxide upon myocardial contractile performance, blood flow and oxygen consumption. *J Physiol* **287**, 149–162.

Wilson, JR., Goldberg, S., Hirshfeld, JW. & Harken, AH. 1981. Effects of respiratory alkalosis on coronary vascular dynamics and myocardial energetics in patients with coronary artery disease. *Am Heart J* **102**, 202-205.

Table 1. Hemodynamics, arterial carbon dioxide tension and pH during $H_2{}^{15}O$ PET studies

| | Rest | Hypercapnea | Hypocapnea |
|---|---|---|---|
| Systolic blood pressure (mmHg) | 146.5 ±20.9 | 159.8 ±25.4 | 144.8 ±26.7 |
| Diastolic blood pressure (mmHg) | 82.8 ±12.0 | 85.3 ±10.7 | 78.5 ±13.2 |
| Heart rate (beat / minute) | 58.4 ±7.8 | 61.6 ±8.7 | 60.7 ±7.8 |
| Rate pressure product | 8472 ±1146 | 9758 ±1609 | 8717 ±1677 |
| Arterial carbon dioxide tension | 40.2 ±2.4 | 43.1 ±2.7* $ | 29.2 ±3.4† $ |
| pH | 7.417 ±0.013 | 7.385 ±0.019 $ | 7.505 ±0.039 $ |

Data are presented as mean ± standard deviation.

Significance of changes compared with the three groups: *P<0.05, †P<0.01 by Fisher PLSD, Significance of changes compared with the resting condition: P<0.05, $ P < 0.01 by Wilcoxon signed rank test

Table 2. Cerebral blood flow ($mL*minute^{-1}*[100\ gram\ of\ perfusable\ tissue]^{-1}$), myocardial blood flow ($mL*minute^{-1}*[100\ gram\ of\ perfusable\ tissue]^{-1}$), and normalized myocardial blood flow ($100mL*mmHg^{-1}*[heart\text{-}beat]^{-1}*[gram\ of\ perfusable\ tissue]^{-1}$)

| | Rest | Hypocapnea | Hypercapnea |
|---|---|---|---|
| Cerebral blood flow | 39.8 ±5.3 | 27.0 ±6.3† | 48.4 ±10.4* |
| Myocardial blood flow | 78.2 ±12.6 | 55.1 ±14.6† | 88.7 ±22.4 |
| Normalized myocardial blood flow | 93.4 ±16.6 | 64.5 ±18.3† | 90.5 ±14.3 |

Significance of changes compared with the three groups: *$P < 0.05$, †$P < 0.01$

ORIGINAL ARTICLE

ACTA RADIOLOGICA

# Comparison of Gd-DTPA-Induced Signal Enhancements in Rat Brain C6 Glioma among Different Pulse Sequences in 3-Tesla Magnetic Resonance Imaging

H. SATO, J. ENMI, N. TERAMOTO, T. HAYASHI, A. YAMAMOTO, T. TSUJI, H. NAITO & H. IIDA

Laboratory for Diagnostic Solutions and Department of Investigative Radiology, Advanced Medical Engineering Center, Research Institute, National Cardiovascular Center, Osaka, Japan; Diagnostic Imaging Medical Affairs, Medical Affairs, Product Development Department, Bayer Yakuhin, Ltd., Osaka, Japan; Department of Radiology, Hospital of National Cardiovascular Center, Osaka, Japan

Sato H, Enmi J, Teramoto N, Hayashi T, Yamamoto A, Tsuji T, Naito H, Iida H. Comparison of gd-dtpa-induced signal enhancements in rat brain c6 glioma among different pulse sequences in 3-tesla magnetic resonance imaging. Acta Radiol 2007;000:1–8.

**Background:** T1-shortening contrast media are routinely used in magnetic resonance (MR) examinations for the diagnosis of brain tumors. Although some studies show a benefit of 3 Tesla (T) compared to 1.5T in delineation of brain tumors using contrast media, it is unclear which pulse sequences are optimal.

**Purpose:** To compare gadopentetate dimeglumine (Gd-DTPA)-induced signal enhancements in rat brain C6 glioma in the thalamus region among different pulse sequences in 3T MR imaging.

**Material and Methods:** Five rats with a surgically implanted C6 glioma in their thalamus were examined. T1-weighted brain images of the five rats were acquired before and after Gd-DTPA administration (0.1 mmol/kg) using three clinically available pulse sequences (spin echo [SE], fast SE [FSE], fast spoiled gradient echo [FSPGR]) at 3T. Signal enhancement in the glioma ($E_T$) was calculated as the signal intensity after Gd-DTPA administration scaled by that before administration. Pulse sequences were compared using the Tukey-Kramer test.

**Results:** $E_T$ was $1.12 \pm 0.05$ for FSE, $1.26 \pm 0.11$ for FSPGR, and $1.20 \pm 0.11$ for SE. FSPGR showed significantly higher signal enhancement than FSE and comparable enhancement to SE.

**Conclusion:** FSPGR is superior to FSE and comparable to SE in its ability to delineate rat brain C6 glioma in the thalamus region.

**Key words:** Brain; contrast agents; MR imaging

*Hiroshi Sato, Laboratory for Diagnostic Solutions, Advanced Medical Engineering Center, Research Institute, National Cardiovascular Center, 5-7-1 Fujishiro-dai, Suita, Osaka 565-8565, Japan (fax. +81 6 6835 5429, e-mail. camo@ri.ncvc.go.jp)*

*Accepted for publication August 5, 2007*

T1-shortening contrast media are routinely used in magnetic resonance (MR) examinations for the diagnosis of brain tumors. Some studies show a benefit of 3 Tesla (T) compared to 1.5T in delineation of brain tumors using contrast media (1–5). However, it is unclear which pulse sequences are optimal. The conventional spin-echo (SE) technique has been most frequently used for T1-weighted (T1W) imaging of tumors after contrast media administration. The gradient-echo (GRE) technique, which is faster than SE, was introduced initially at 1.5T or lower field strength (6–11). Some studies have reported that GRE techniques compare favorably with the SE technique for delineation of brain tumors (8–10), while other studies have reported that GRE techniques do not show contrast enhancement as well as SE (6, 7, 11). At 3T, as at 1.5T or lower field strength, the issue of whether GRE techniques are effective compared to SE has not been determined. In 16 patients, NÖBAUER-HUMANN et al. reported that 3D GRE with magnetization preparation (MPRAGE) was comparable to T1W SE in tumor-to-brain contrast at 3T, although the parameters of T1W SE were not

informa
healthcare

DOI 10.1080/02841850701630326 

optimized for 3T (1). In 12 patients, FISCHBACH et al. compared four T1W sequences: SE, inversion recovery fast SE (IR-FSE), 2D GRE, and MPRAGE at 3T. They observed that SE and IR-FSE provided higher contrast enhancement of brain tumors than 2D GRE and MPRAGE. Furthermore, their impressions showed that the visual quality of SE was superior to that of the other three sequences (12).

In order to compare pulse sequences, it would be preferable if the pathological and physiological conditions of subjects were constant across scans. One possible model system is the widely used rat brain glioma model (4, 5, 13–15). In most studies with small animals, MR imaging systems with small magnets are widely used. The pulse sequences available on the scanner designed for small animals, however, are different from those on a clinical scanner. By using a scanner designed for humans, we can compare diagnostic values of practical clinical pulse sequences. To our knowledge, no studies have been reported comparing pulse sequences on a 3T human scanner using a rat brain glioma model.

The purpose of the current study was to elucidate the optimal pulse sequence that provides the highest obtainable signal enhancement using gadopentetate dimeglumine (Gd-DTPA) in a rat brain C6 glioma model on a 3T human whole-body scanner.

## Material and Methods

Protocols of all animal procedures were approved by the ethics committee for animal research at the National Cardiovascular Center. Male Sprague-Dawley rats (Japan SLC, Inc., Shizuoka, Japan) were used. Rats had free access to food and water, and were kept in uncrowded conditions (two/cage) in a light-, temperature-, and humidity-regulated room (light on 07.00–19.00, $23 \pm 3$°C, and $50 \pm 20$%).

### *Study design*

T1 measurements in the brains of three normal rats and phantom studies were performed to identify pulse sequences, among which Gd-DTPA-induced signal enhancements in rat C6 brain gliomas were compared, and to determine pulse sequence parameters. Using the determined pulse sequences and parameters, we examined five rats with developed gliomas out of 20 rats that received C6 glioma implantation in their thalamus region.

### *MR imaging system*

All scanning was performed on a 3T whole-body scanner (Signa LX VH3M4; GE Healthcare, Milwaukee, Wisc., USA) equipped with the manufacturer's gradient system (maximum gradient strength 40 mT/m; slew rate 150 mT/m/s).

For imaging rat brains, we built a three-turn solenoid coil with a diameter of 42 mm and a length along the cylindrical axis of 18 mm. The diameter and length of this coil were adjusted to rat head size. The helical pitch of the coil was wide enough to pass the ear bars used to secure the rat's head. The coil was capable of transmission and reception, and was tuned to an impedance of 50 Ω at a resonant frequency of 127.76 MHz. Capacitance was divided into six elements in series, which were put at each half turn. The coil was mounted on a fixing apparatus (Narishige Co., Ltd., Tokyo, Japan) using an acrylic jig specially designed for the coil (Fig. 1). Rats were placed prone on the fixing apparatus. Rat heads were secured using an incisor hook and ear bars. All components of the fixing apparatus consisted of non-magnetic materials. During imaging, the fixing apparatus, on which the rat and the coil were mounted, was placed in the gantry so that the cylindrical axis of the coil and the cranial-to-caudal direction of the rat were perpendicular to a static magnetic field, and the center of the rat brain was positioned at the magnet isocenter.

### *Measurement of T1 in normal rat brain*

This measurement was performed to establish the normal T1 value in the transplantation site (thalamus) of the C6 glioma cells. T1 values in the brain of three normal rats (9–13 weeks old, $380 \pm 50$ g) were

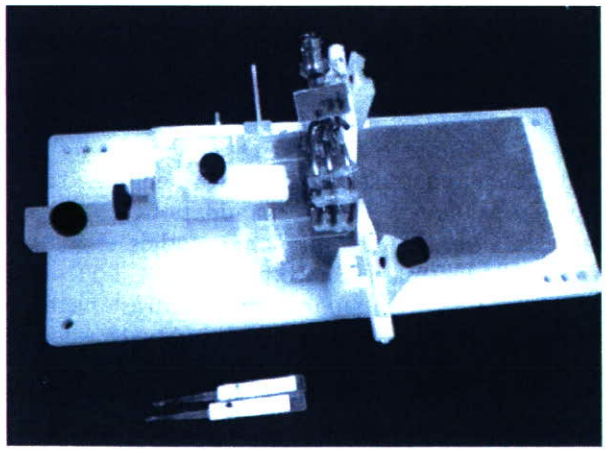

Fig. 1. The three-turn solenoid coil and the fixing apparatus used for the imaging of rats in the present study. The coil was mounted on the fixing apparatus using the specially designed acrylic jig.



Acta Radiologica rad134548.3d 23/10/07 20:33:23
The Charlesworth Group, Wakefield +44(0)1924 369598 - Rev 7.51n/W (Jan 20 2003)
262880

measured by using a saturation recovery method with a variable repetition time (TR) SE imaging sequence (16): TR 600, 1000, 2000, 4000, 8000 ms; echo time (TE) 10 ms; bandwidth (BW) 16 kHz; field of view (FOV) 40 × 30 mm; matrix size 256 × 160; slice thickness 1 mm; slice gap 1 mm; number of slices 16; number of excitations (NEX) 1; coronal plane. An 8-cm polyvinyl chloride tube with an outer diameter of 2.7 mm was inserted into the animal's trachea, and the rats were ventilated with an average of 2–3 ml per breath of a mixture of $O_2$, $N_2$, and air (2:1:10) using a small animal ventilator (CWE SAR-830/AP Ventilator; CWE, Inc., Ardmore, Pa., USA) at an average of 80 breaths per minute. Body temperature was monitored rectally (36.0 ± 0.5°C).

T1 values were estimated on a pixel-by-pixel basis using the non-linear least-square fit of the signal intensity measured for each TR value. In the obtained T1 images, regions of interest (ROIs) were placed on the thalamus, hippocampus, olfactory bulb, cerebral cortex, corpus callosum, midbrain, cerebellum, pons, cerebrospinal fluid, and muscle. Mean T1 values were calculated from each ROI. A mean and a standard deviation of the mean values obtained from three rats were calculated.

*Phantom study*

*Phantom preparation.* Gd-DTPA (Magnevist; Bayer Schering Pharma, Osaka, Japan) was diluted with saline to obtain 19 solutions with different concentrations (0, 0.01, 0.03, 0.05, 0.07, 0.1, 0.15, 0.2, 0.25, 0.3, 0.5, 0.7, 1, 3, 5, 7, 10, 30, and 50 mM). Each solution was encapsulated in separate polypropylene vials with a diameter of 27 mm, which were set in agar.

*T1 measurement.* T1 values of each Gd-DTPA solution were measured at room temperature using the same pulse sequence as the T1 measurement in normal rats: TR 34, 100, 200, 400, 600, 800, 1000, 1200, 1400, 1600, 1800, 2000, 4000, 6000, 8000, 11,000, 15,000 ms; TE 9 ms; BW 16 kHz; FOV 210 × 158 mm; matrix size 256 × 192; slice thickness 3 mm; number of slices 1; NEX 1. A standard quadrature birdcage head coil was used.

Circular ROIs with 70–80% of the diameter of a vial were placed on a homogeneous signal portion of each phantom image. T1 values were estimated by non-linear least-square fit of the average signal intensity of all voxels in the ROI measured for each TR value. Five measurements were performed for phantoms, and the mean and standard deviation of measured T1 values were calculated.

*Choice of pulse sequences.* We used a Gd-DTPA saline solution (0.1 mM) with a T1 value close to that in the normal thalamus as a corresponding solution to the glioma in the thalamus region before contrast. We hypothesized that T1 in the glioma would not be so different from that in normal tissue. Saline solutions with a higher concentration of Gd-DTPA were regarded as a corresponding solution to the glioma after contrast.

T1W images of each phantom were acquired at room temperature (approximately 21°C) using four clinically available pulse sequences (SE, fast SE [FSE], IR-FSE [T1FLAIR], and fast spoiled GRE [FSPGR]) (Table 1). A standard quadrature birdcage head coil was used for the imaging of phantoms.

Circular ROIs with 70–80% of the diameter of the vial were placed on a uniform signal portion of each phantom. Mean signal intensities were calculated from each ROI. For each sequence, signal enhancements of each Gd-DTPA solution ($E_P$) were calculated as $E_P = S/S_0$, where S is the signal intensity of each solution and $S_0$ is that of 0.1 mM of the solution. The pulse sequences showing high $E_P$ were used for the imaging of C6 glioma model rats and were compared based on Gd-DTPA-induced signal enhancements in brain tumors, delineated by histopathology.

*Rat brain C6 glioma model study*

*Preparation of rat brain C6 glioma models.* C6 glioma cells (CCL-107 cell line, ATCC; Summit Pharmaceuticals International Corporation, Tokyo,

Table 1. Pulse sequences and imaging parameters used for imaging of saline phantoms containing gadopentetate dimeglumine (Gd-DTPA)

| Pulse sequence | TR, ms | TE, ms | TI, ms | FA, ° | ETL | BW, kHz | NEX | Acquisition time, min:s |
|---|---|---|---|---|---|---|---|---|
| SE | 1400 | 14 | — | — | — | 16 | 1 | 4:46 |
| FSE | 1400 | 16 | — | — | 3 | 32 | 1 | 1:52 |
| T1FLAIR | 3000 | 16 | 1300 | — | 3 | 32 | 1 | 4:00 |
| FSPGR | 20 | 3.2 | — | 30 | — | 32 | 10 | 0:39 |

For all pulse sequences, FOV was 210 × 158 mm, matrix was 256 × 192, the number of slices was 1, and the slice thickness was 3 mm. SE: spin echo; FSE: fast spin echo; T1FLAIR: inversion recovery fast spin echo; FSPGR: fast spoiled gradient echo; TR: repetition time; TE: echo time; TI: inversion time; FA: flip angle; ETL: echo train length; BW: bandwidth; NEX: number of excitations.



**Acta Radiologica rad134548.3d** 23/10/07 20:33:24
*The Charlesworth Group*, Wakefield +44(0)1924 369598 - Rev 7.51n/W (Jan 20 2003)
**262880**

Japan) were implanted into the region of the thalamus in the left hemispheres of the brains of 20 rats (8 weeks old, 292.8±14.8 g). The implantation procedures were performed under general anesthesia using an intramuscular injection of ketamine (33 mg/kg; Sankyo Co., Ltd., Tokyo, Japan) and xylazine (7 mg/kg; Bayer AG, Leverkusen, Germany). A burr hole was made 3 mm lateral and 2 mm posterior to the bregma using a dental drill. A needle with an outer diameter of 0.3 mm was inserted 4 mm below the outer table of the skull through the burr hole. A 10-$\mu$l solution containing $10^7$ cells/ml was infused over 5 min at a constant rate using a microsyringe (Hamilton Co., Reno, Nev., USA) and infusion pump (Eicom Corp., Kyoto, Japan).

*MR imaging.* Two weeks after implantation, all 20 rats underwent screening by T1W imaging after Gd-DTPA administration. Developed glioma was confirmed in only five out of 20 rats. Those five rats were used for experiments for the comparison of pulse sequences. Three weeks after implantation, when the glioma was fully developed, T1W brain images of the selected five rats (11 weeks old, 301.3±29.0 g) were acquired before and after Gd-DTPA administration using three pulse sequences determined by the phantom study (Table 2) in the coronal plane. Rats were given general anesthesia with an intramuscular injection of a ketamine (33 mg/kg) and xylazine (7 mg/kg) mixture, and allowed to breathe spontaneously during preparation and imaging. First, precontrast T1W images were acquired. Then, a dose of 0.1 mmol/kg of Gd-DTPA was administered by hand injection followed by a 3.0-ml saline flush through a 22G indwelling needle placed in a tail or femoral vein. Postcontrast T1W imaging started 1 min after Gd-DTPA administration with identical settings to the precontrast imaging. Each rat was examined using all three pulse sequences (Table 2). In order to eliminate the effect of previously administered Gd-DTPA, three scans using different pulse sequences were performed on three separate days, at 22- to 26-hour intervals, in a randomized order.

*ROI analysis.* Based on the results of histopathology (see below), ROIs were placed on a portion of each glioma. Areas of necrosis or hemorrhage were excluded from the ROI. Mean signal intensities in the pre- and postcontrast T1W images were calculated from each ROI. For each sequence, signal enhancement of each glioma ($E_T$) was calculated as $E_T=S_{post}/S_{pre}$, where $S_{post}$ is signal intensity in the glioma after contrast and $S_{pre}$ is that before contrast.

*Histopathology*

One day after MR imaging, rat brains were removed and fixed in formalin. All brains were completely coronally sectioned. Sections were stained with hematoxylin and eosin (HE) in order to delineate areas of glioma, hemorrhage, and necrosis.

*Statistical analysis*

All parameters assessed were given as means ± standard deviations. Pair-wise comparison among pulse sequences was performed using the Tukey-Kramer test. A $P$ value of $<0.05$ was considered statistically significant.

## Results

*T1 in normal rat brains*

Fig. 2 shows images from one of the three normal rats used to quantitate T1 values in the brain. Table 3 summarizes the T1 values of typical brain structures. The T1 value in the thalamus was 1405±32 ms.

*T1 of Gd-DTPA solutions*

Fig. 3 shows selected images from a series of 17 images obtained with different TR values. Table 4 summarizes T1 values in the Gd-DTPA solutions

Table 2. Pulse sequences and imaging parameters used for imaging of rat brains with C6 glioma cell implants

| Pulse sequence | TR, ms | TE, ms | FA, ° | ETL | BW, kHz | NEX | Acquisition time, min:s |
|---|---|---|---|---|---|---|---|
| SE | 1400 | 13 | — | — | 16 | 1 | 4:46 |
| FSE | 1400 | 18.6 | — | 3 | 32 | 3 | 4:32 |
| FSPGR | 20 | 4.7 | 30 | — | 32 | 8 | 5:40 |

For all pulse sequences, FOV was 60 × 45 mm, matrix was 256 × 192, the number of slices was 11, and the slice thickness was 2.5 mm (0.5-mm gap). SE: spin echo; FSE: fast spin echo; FSPGR: fast spoiled gradient echo; TR: repetition time: TE: echo time; FA: flip angle; ETL: echo train length; BW: bandwidth; NEX: number of excitations.



Acta Radiologica rad134548.3d 23/10/07 20:33:24
The Charlesworth Group, Wakefield +44(0)1924 369598 - Rev 7.51n/W (Jan 20 2003)
262880

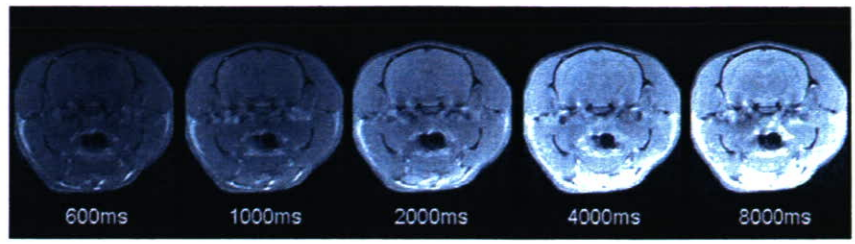


Fig. 2. Images from one of three rats used for the measurement of T1 values in normal rat brain. One of 16 slices acquired is shown. The images are arranged from left to right in ascending order of repetition time. All five images are set with equal window width and equal window level.

Table 3. T1 relaxation time in normal rat brain at 3T

| | T1, ms |
|---|---|
| Thalamus | 1405 ± 32 |
| Hippocampus | 1779 ± 151 |
| Olfactory bulb | 1613 ± 117 |
| Cerebral cortex | 1506 ± 13 |
| Corpus callosum | 1389 ± 43 |
| Midbrain | 1329 ± 50 |
| Cerebellum | 1726 ± 356 |
| Pons | 1343 ± 80 |
| Cerebrospinal fluid | 3460 ± 737 |
| Muscle | 1529 ± 99 |

Mean and standard deviation of values obtained from three rats.

ranging from 0 to 10 mM. In 30 and 50 mM solutions, an accurate T1 value could not be measured because of extensive signal loss due to T2 decay. The 0.1-mM solution showed a T1 value (1302 ± 54 ms) closest to that in the normal thalamus (1405 ± 32 ms).

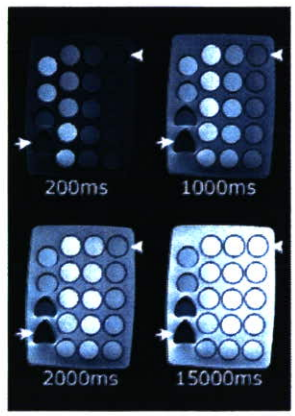


Fig. 3. Images obtained in the measurement of T1 values of 19 saline solutions with different concentrations of gadopentetate dimeglumine (0, 0.01, 0.03, 0.05, 0.07, 0.1, 0.15, 0.2, 0.25, 0.3, 0.5, 0.7, 1, 3, 5, 7, 10, 30, and 50 mM). The four selected images from a series of 17 images obtained with different TR values are shown. Each solution was encapsulated in separate polypropylene vials, which were set in agar. The concentration of gadopentetate dimeglumine decreases from bottom to top and from left to right. Arrows and arrowheads denote the 50-mM and 0-mM solutions, respectively. All four images are set with equal window width and equal window level.

Table 4. T1 of saline with different concentrations of Gd-DTPA at 3T

| Gd-DTPA concentration, mM | T1, ms |
|---|---|
| 0 | 3026 ± 121 |
| 0.01 | 2652 ± 96 |
| 0.03 | 2245 ± 108 |
| 0.05 | 1970 ± 92 |
| 0.07 | 1775 ± 103 |
| 0.1 | 1302 ± 54 |
| 0.15 | 993 ± 57 |
| 0.2 | 820 ± 52 |
| 0.25 | 737 ± 51 |
| 0.3 | 666 ± 63 |
| 0.5 | 389 ± 17 |
| 0.7 | 284 ± 12 |
| 1 | 209 ± 9 |
| 3 | 84 ± 4 |
| 5 | 58 ± 2 |
| 7 | 36 ± 1 |
| 10 | 27 ± 1 |
| 30 | — |
| 50 | — |

Mean and standard deviation of values obtained from five measurements.

*Choice of pulse sequences*

Fig. 4 shows $E_P$ in the Gd-DTPA solutions ranging from 0.1 to 50 mM. In Gd-DTPA solutions ranging from 0.15 to 30 mM, a higher $E_P$ was obtained as follows: FSPGR > SE > FSE > T1FLAIR. Because $E_P$ for T1FLAIR was lowest at all concentrations, T1FLAIR was not used for the imaging of rat brain tumors.

Based on our preliminary experiments, the T1 value in the glioma in the thalamus region after contrast was about 90% of that before contrast. Therefore, we regarded the 0.15-mM solution as a corresponding solution to glioma after contrast, and compared $E_P$ values at 0.15 mM obtained using different sequences (Fig. 5). $E_P$ at 0.15 mM was 1.10 ± 0.02 for FSE, 1.16 ± 0.01 for FSPGR, 1.16 ± 0.01 for SE, and 1.06 ± 0.01 for T1FLAIR. The Tukey-Kramer test showed significant differences ($P < 0.05$) between all pairs except for FSPGR–SE. $E_P$ for FSPGR was significantly higher than that for FSE and T1FLAIR and comparable to that for SE.



**Acta Radiologica rad134548.3d** 23/10/07 20:33:24
*The Charlesworth Group*, Wakefield +44(0)1924 369598 - Rev 7.51n/W (Jan 20 2003)
**262880**

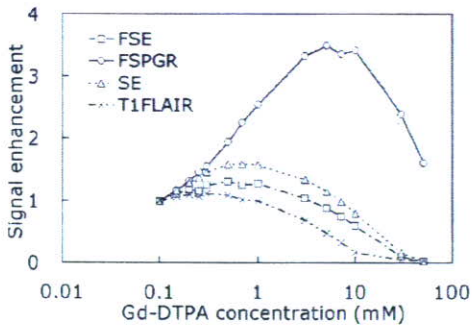


Fig. 4. Signal enhancements in saline solutions containing gadopentetate dimeglumine (Gd-DTPA) obtained by the following pulse sequences: spin echo (SE); fast spin echo (FSE); inversion recovery fast spin echo (T1FLAIR); fast spoiled gradient echo (FSPGR). Signal enhancement was the signal intensity scaled by that of a 0.1-mM Gd-DTPA solution whose T1 value was closest to the average T1 value in the brain parenchyma of normal rats.

*Signal enhancement in rat brain C6 glioma*

Fig. 6 displays typical pre- and postcontrast T1W images of brains of C6 glioma model rats, together with an example of ROIs placed on the glioma and HE-stained slices. Fig. 7 shows the comparison between $E_T$ values for FSE, SE, and FSPGR. $E_T$ values were $1.12 \pm 0.05$ for FSE, $1.26 \pm 0.11$ for FSPGR, and $1.20 \pm 0.11$ for SE. The Tukey-Kramer test showed the significant superiority of FSPGR over FSE. There was no significant difference between FSPGR and SE.

## Discussion

T1W imaging using SE results in a corresponding restriction in the number of slices as a result of the

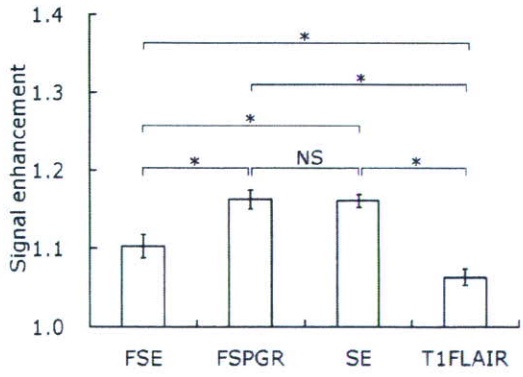


Fig. 5. Signal enhancement of saline solution with 0.15 mM Gd-DTPA obtained using different pulse sequences: spin echo (SE); fast spin echo (FSE); inversion recovery fast spin echo (T1FLAIR); fast spoiled gradient echo (FSPGR). Signal enhancement was defined as the signal intensity of a 0.15-mM solution scaled by that of a 0.1-mM solution. The Tukey-Kramer test was performed for pair-wise comparison among four pulse sequences. The asterisk and NS denote significant difference ($P < 0.05$) and no significant difference ($P > 0.05$), respectively.

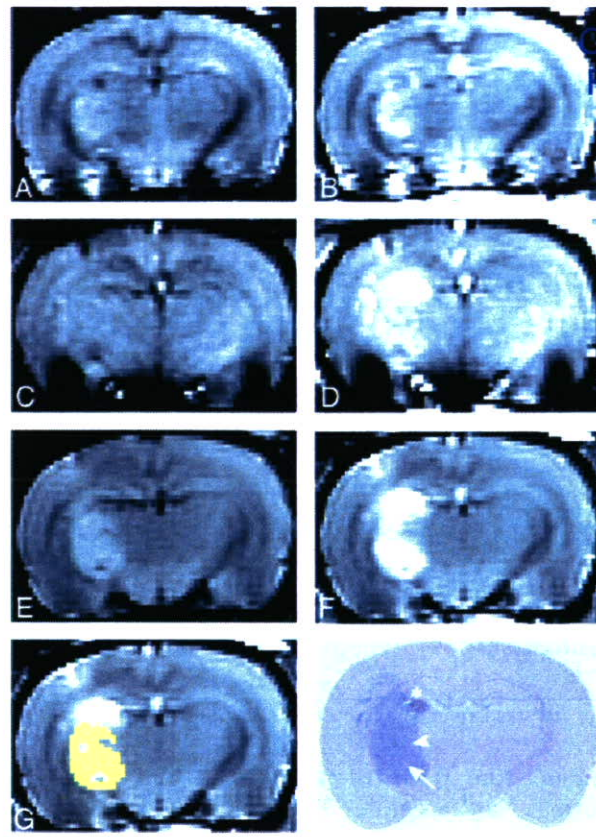


COLOUR FIGURE

Fig. 6. Examples of pre- (A, C, E) and post-contrast (B, D, F) coronal T1-weighted images obtained using fast spin-echo (FSE) (A, B), fast spoiled gradient-echo (FSPGR) (C, D), and spin-echo (SE) (E, F) sequences. A region of interest (ROI) placed on the glioma (G) and a slice stained using hematoxylin and eosin (HE) (H). T1-weighted images were acquired 3 weeks after the implantation of C6 glioma cells. Areas of necrosis or hemorrhage, which were delineated based on histopathology, were excluded from ROIs. In the HE-stained slice, small-cell glioma (arrowhead), hemorrhage (asterisk), and necrosis (arrow) were found.

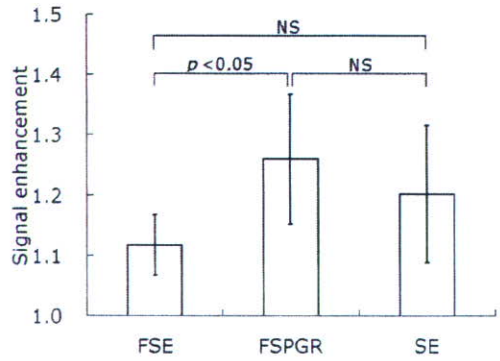


Fig. 7. Signal enhancement in rat brain C6 glioma obtained with different pulse sequences: spin echo (SE); fast spin echo (FSE); fast spoiled gradient echo (FSPGR). Signal enhancement was defined as the signal intensity after Gd-DTPA administration scaled by that before administration. The pair-wise comparison among pulse sequences was performed using the Tukey-Kramer test. NS denotes no significant difference ($P > 0.05$).



Acta Radiologica rad134548.3d 23/10/07 20:33:27
The Charlesworth Group, Wakefield +44(0)1924 369598 - Rev 7.51n/W (Jan 20 2003)
262880

specific absorption rate (SAR) at 3T. The use of FSE makes radiofrequency heating more serious. Compared to SE and FSE, FSPGR provides relatively low radiofrequency heating and, if the NEX of FSPGR can be reduced, relatively short acquisition time. This depends on the signal-to-noise ratio, and we thought it possible based on our rat brain images (Fig. 6). Therefore, we examined the characteristics of signal enhancement in FSPGR. FSPGR provided significantly higher signal enhancement than FSE and comparable signal enhancement to SE, both in the 0.15-mM Gd-DTPA solution and in rat brain C6 glioma in the thalamus region. We speculate that FSPGR may be superior to FSE and comparable to SE in its ability to delineate brain tumors, although, in order to verify this speculation, several studies would be required using different cell types and various transplantation sites. Considering the advantage of FSPGR in terms of acquisition time and SAR limit, FSPGR may be more suitable for contrast-enhanced T1W imaging of brain tumors in clinical 3T scanners than SE. Additionally, high-resolution 3D images can be obtained by using FSPGR with a reasonable acquisition time so that small lesions may be better visualized. On the other hand, FSPGR was more sensitive to magnetic susceptibility artifacts than SE (Fig. 6). SE could therefore be more suitable than FSPGR for delineation of tumors in regions with susceptibility artifacts, such as the base of the skull.

$E_T$ values obtained in our study (1.26 for FSPGR, 1.20 for SE, and 1.12 for FSE) were lower compared to previously reported values (1, 4, 5, 12). For example, RUNGE et al. reported that the $E_T$ induced by Gd-DTPA was approximately 1.44 using SE in rat brain C6/LacZ glioma models at 3T (5). The difference between $E_T$ in our study and that in previous reports may result from the difference in the type of tumor, in the degree of growth of brain tumors, or in TR. In our study, TR was adjusted to increase T1 contrast in the normal brain region for specification of more exact location of the glioma. Although the use of a shorter TR may increase signal enhancement in the glioma, contrast in the normal region would become unclear, and therefore it could become difficult to specify the location of the glioma exactly. Therefore, we used a longer TR than that in previous reports.

FISCHBACH et al. showed higher contrast in SE in patients, but they optimized the TR (600 ms) of SE by phantom experiments using a saline solution with a low concentration of Gd-DTPA (0.125 $\mu$M) (12), whose T1 is extremely long compared to that in the brain. We quantified T1 in rat brains and chose a proper TR (1400 ms) of SE to enhance normal brain contrast. Therefore, our comparison would be fairer and our results may be more closely extrapolated to human tumors.

One limitation of our work is our limited sample size. Although C6 glioma cells were implanted into 20 rats in our in-vivo study, only five rats could be used for the experiment, as C6 gliomas showed considerable individual variation in their growth and were fully developed only in five rats. Therefore, the number of test animals was relatively small, resulting in large standard deviations for $E_T$. A larger sample size may show a significant difference between FSPGR and SE.

In conclusion, FSPGR is superior to FSE and comparable to SE in its ability to delineate rat brain C6 glioma in the thalamus region using venous injection of Gd-DTPA.

## Acknowledgments

This study was supported by a research grant on Advanced Medical Technology from the Ministry of Health, Labor and Welfare (MHLW), Japan (H17-nano-15), and a Program for Promotion of Fundamental Studies in Health Science of the Organization for Pharmaceutical Safety and Research (of Japan) Health Science Research Grant (H13-005) from the Ministry of Health, Labor and Welfare, (of Japan)

## References

1. Nöbauer-Huhmann IM, Ba-Ssalamah A, Mlynarik V, Barth M, Schoggl A, Heimberger K, et al. Magnetic resonance imaging contrast enhancement of brain tumors at 3 tesla versus 1.5 tesla. Invest Radiol 2002;37:114–9.
2. Trattnig S, Ba-Ssalamah A, Noebauer-Huhmann IM, Barth M, Wolfsberger S, Pinker K, et al. MR contrast agent at high-field MRI (3 Tesla). Top Magn Reson Imaging 2003;14:365–75.
3. Ba-Ssalamah A, Nöbauer-Huhmann IM, Pinker K, Schibany N, Prokesch R, Mehrain S, et al. Effect of contrast dose and field strength in the magnetic resonance detection of brain metastases. Invest Radiol 2003;38:415–22.
4. Biswas J, Nelson CB, Runge VM, Wintersperger BJ, Baumann SS, Jackson CB, et al. Brain tumor enhancement in magnetic resonance imaging: comparison of signal-to-noise ratio (SNR) and contrast-to-noise ratio (CNR) at 1.5 versus 3 tesla. Invest Radiol 2005;40: 792–7.
5. Runge VM, Biswas J, Wintersperger BJ, Baumann SS, Jackson CB, Herborn CU, et al. The efficacy of gadobenate dimeglumine (Gd-BOPTA) at 3 Tesla in brain magnetic resonance imaging: comparison to 1.5

Tesla and a standard gadolinium chelate using a rat brain tumor model. Invest Radiol 2006;41:244–8.
6. Chappell PM, Pelc NJ, Foo TK, Glover GH, Haros SP, Enzmann DR. Comparison of lesion enhancement on spin-echo and gradient-echo images. Am J Neuroradiol 1994;15:37–44.
7. Rand S, Maravilla KR, Schmiedl U. Lesion enhancement in radio-frequency spoiled gradient-echo imaging: theory, experimental evaluation, and clinical implications. Am J Neuroradiol 1994;15:27–35.
8. Pui MH, Fok EC. MR imaging of the brain: comparison of gradient-echo and spin-echo pulse sequences. Am J Roentgenol 1995;165:959–62.
9. Fellner F, Holl K, Held P, Fellner C, Schmitt R, Bohm-Jurkovic H. A T1-weighted rapid three-dimensional gradient-echo technique (MP-RAGE) in preoperative MRI of intracranial tumours. Neuroradiology 1996;38: 199–206.
10. Li D, Haacke EM, Tarr RW, Venkatesan R, Lin W, Wielopolski P. Magnetic resonance imaging of the brain with gadopentetate dimeglumine-DTPA: comparison of T1-weighted spin-echo and 3D gradient-echo sequences. J Magn Reson Imaging 1996;6:415–24.
11. Elster AD. How much contrast is enough? Dependence of enhancement on field strength and MR pulse sequence. Eur Radiol 1997;7 Suppl 5:276–80.
12. Fischbach F, Bruhn H, Pech M, Neumann F, Ricke J, Felix R, et al. Efficacy of contrast medium use for neuroimaging at 3.0 T: utility of IR-FSE compared to other T1-weighted pulse sequences. J Comput Assist Tomogr 2005;29:499–505.
13. Raila FA, Bowles AP Jr, Perkins E, Terrell A. Sequential imaging and volumetric analysis of an intracerebral C6 glioma by means of a clinical MRI system. J Neurooncol 1999;43:11–7.
14. Thorsen F, Ersland L, Nordli H, Enger PO, Huszthy PC, Lundervold A, et al. Imaging of experimental rat gliomas using a clinical MR scanner. J Neurooncol 2003;63:225–31.
15. Blanchard J, Mathieu D, Patenaude Y, Fortin D. MR-pathological comparison in F98-Fischer glioma model using a human gantry. Can J Neurol Sci 2006;33: 86–91.
16. Wansapura JP, Holland SK, Dunn RS, Ball WS Jr. NMR relaxation times in the human brain at 3.0 tesla. J Magn Reson Imaging 1999;9:531–8.



**Acta Radiologica** **rad134548.3d** 23/10/07 20:33:45
*The Charlesworth Group*, Wakefield +44(0)1924 369598 - Rev 7.51n/W (Jan 20 2003)
**262880**